RSC Advances

PAPER

View Article Online
View Journal | View Issue

Cite this: *RSC Adv.*, 2026, **16**, 3965

Enhancing the sensitivity of nanobodies through covalent and non-covalent polymerization

Feng Wang, *[ab] Jun Chen,[b] Jing-Hua Chen,[b] Xue-Mei Liu,[b] Li-Qiao Hu[b] and Li-Jun Huo*[a]

Received 23rd May 2025
Accepted 29th December 2025

DOI: 10.1039/d5ra03619d

rsc.li/rsc-advances

The precise identification of disease using antibodies is crucial for guiding therapeutic interventions. Among these binding proteins, the nanobody is the smallest known antigen-binding fragment. This study aimed to enhance antigen detection sensitivity by integrating covalent dimerization and non-covalent heptamerization strategies to increase the density of nanobodies for improved antigen capture. First, we synthesized a SpyTag-Catcher-fused nanobody and a heptamerization protein using a prokaryotic expression system. Western blot was used to preliminarily verify the nanobody's antigen-binding capability. Surface Plasmon Resonance (SPR) analysis revealed that the enhanced immunoactivity of the nanobody polymerization resulted from their increased affinity. Finally, we employed these nanobodies to improve the sensitivity of sandwich immunoassays, specifically immuno-magnetic beads and ELISA, for detecting antigens in solution. Our findings demonstrate that the 14-mer nanobody, formed by covalent dimers and non-covalently self-assembled heptamers, enhanced antigen capture capability by more than tenfold.

1 Background

Precise disease diagnosis is essential for early detection and for optimizing clinical treatment. Traditional Y-shaped antibodies have been extensively used in scientific research, diagnostics, and therapeutics. However, the large size of conventional antibodies limits opportunities for sequence modification, complicates their expression, and restricts their application *in vivo*.

In camelids, first identified antibodies consisting of only heavy chains.[1] These heavy-chain-only antibodies lack light chains and the first constant region (CH1). They bind to antigens solely through the variable region of the heavy chain.[2] This structure is similar in both sequence and conformation to the VH domain of human IgG3.[3] Analogous antibodies were subsequently discovered in cartilaginous fish, including sharks and rays.[4] The variable domain of these heavy-chain antibodies measures 4 × 2.5 nm and has a molecular weight of 12–15 kD,[5] making it the smallest known antigen-binding protein. This fragment, known as a nanobody, is approximately one-tenth the size of a conventional antibody. Nanobodies can be produced cost-effectively at a large scale in *E. coli*. Compared to traditional antibodies, they offer significant advantages, including high editability, solubility, binding affinity, stability, and specificity. Their small size facilitates genetic engineering, library screening, protein purification, and access to hidden epitopes that are often challenging for conventional antibodies to recognize.[6,7] As a result, nanobodies are increasingly being employed to treat various diseases and identify pathogens.[8,9]

In contrast to IgG antibodies, which have been successfully used in clinical practice for decades, nanobodies remain a nascent and largely unexplored area of research. Although nanobodies exhibit high stability and solubility,[10] their monovalent interaction with antigens often results in insufficient affinity for detection systems.[11] To address this limitation, polymerization strategies are employed to enhance the detection sensitivity of nanobodies.[12] One approach involves engineering macromolecular polymeric antibodies to replicate the characteristics of pentameric IgM,[13] which plays a key role in the initial stage of hyperacute immunological rejection in mammals. For instance, Uchański *et al.* generated large antibody constructs by conjugating nanobodies to pentameric scaffold proteins *via* fusion expression,[14] enabling the stable and efficient production of polymeric proteins. Polymerization methods include domain switching,[15] transpeptidation, fusion expression, covalent chemical ligation[16] (using tools such as inteins[17] and sortase[18]), and non-covalent interactions (such as self-associating peptides[19] and streptavidin–biotin systems[20]).

C4bp (also known as IMX313) is an abundant plasma protein first identified in mice.[21] The C4BP scaffold used in our study is a hybrid derived from the original chicken heptamerizing oligomerization coiled-coil.[22] Separately, Zakeri *et al.* developed a rapid covalent linkage system based on a protein from *S.*

[a]*Biomedical Research Institute, Hubei University of Medicine, Shiyan 442000, Hubei, China. E-mail: wangfeng86147545@163.com; ljhuo@hbmu.edu.cn*

[b]*Department of Testing and Diagnosis Technology Research, Guangzhou National Laboratory, Guangzhou, Guangdong, China*

dysgalactiae,[23] which forms spontaneous isopeptide bonds for irreversible protein conjugation. This system consists of a peptide tag (SpyTag) and its binding partner (SpyCatcher),[24] representing a significant advance for protein engineering. We implemented the SpyTag/Catcher protein ligation system,[25] along with the SnoopTag/Catcher system, which can be used in conjunction with SpyTag/Catcher to enable flexible modular assembly.[26] In the heptameric C4BP structure, which resembles an octopus, the N-terminal is located at the top.[27] C4BP contains an amphipathic helix and two cysteine residues,[28] forming a self-associating, spider-like heptameric protein[29] capable of linking seven VHH domains and seven biotin molecules at its protein terminus (RCSB database: 4B0F).[30]

To advance the development of recombinant nanobodies for antigen, we aimed to create a highly sensitive, self-assembling nanobody platform. This was achieved by combining COVID-19 nucleocapsid protein-specific nanobodies[31] with heptameric C4BP scaffold proteins.[32] The design links seven covalently bonded N-terminal VHH dimers to a non-covalent, self-assembled C4BP heptamer, forming a 14-mer megamolecular complex to significantly enhance nanobody sensitivity (Fig. 1). This megamolecular system represents a versatile and modular platform for engineering high-avidity nanobody displays.

2 Method

Anti-HIS tag antibody, LB medium, isopropyl alcohol, *b*-D-1-thiogalactopyranoside (IPTG), and all buffer salts were obtained from Shanghai Sangon. Nickel Sepharose high-performance resin, prepacked columns, and Superdex 200 size exclusion chromatography columns were obtained from Cytiva. All restriction enzymes and cloning buffers were obtained from Thermo Fisher (MA, USA). The prokaryotic expression vector pET22b and all primers (Table S1) were obtained from Guangzhou Ruibo Xingke.

2.1 Prokaryotic expression and purification of nanobodies

Escherichia coli is the most widely used system for recombinant protein production. To express nanobodies, the coding sequences were cloned into the pET22b vector with an N-terminal PelB signal peptide (22 amino acids, 2.2 kD) to direct secretion into the oxidative environment of the periplasm, which facilitates correct folding and disulfide bond formation. The nanobodies used in this study are specific to the COVID-19 nucleocapsid protein. Dimeric nanobodies were constructed by linking two VHH domains with a 3× (GGGGS) linker. The recombinant nanobody genes were cloned into the pET22b vector and verified by DNA sequencing (Table S2 and Fig. S1). The confirmed plasmids were transformed into *E. coli* BL21 (DE3) cells. Protein expression was induced in competent cells grown in ampicillin (100 μg mL^{-1}) with 1 mM IPTG at 16 °C for 16 hours. Nanobodies were released from the periplasmic space by osmotic shock. The resulting lysate was purified using a Ni-NTA affinity column to isolate the 6× His-tagged nanobodies. The molecular weight and purity of purified nanobodies were analyzed by a 15% SDS-PAGE (PAGE Gel Rapid Preparation Kit, Shanghai Yase Biotechnology Co., Ltd, PG114) (Fig. S2). The nanobodies constructs included the PelB leader sequence, VHH domains, 3C protease site, sortase recognition motif, SpyTag, and 6× His tags (B6: 189 amino acids, 20 kD; C2: 183 amino acids, 20 kD; E2: 188 amino acids, 21 kD; see Fig. S1 and Table S2). The dimeric nanobody proteins consisted of two VHH domains connected by a linker, and contained restriction sites, SpyTag, sortase sites, and 6× His tags (C2–B6: 331 amino acids, 35 kD; E2–E2: 334 amino acids, 36 kD). SDS-PAGE analysis with Coomassie Brilliant Blue staining confirmed that the purified nanobodies were distinct, pure, and free of degradation. The purified samples were flash-frozen in liquid nitrogen and stored at −80 °C for long-term preservation.

2.2 Western blotting and Coomassie brilliant blue staining

For western blot analysis, 5 μg of COVID-19 nucleocapsid protein antigen was mixed with protein loading buffer. The sample, along with a protein ladder (26 619, PageRuler, Thermo Fisher Scientific, MA, USA), was loaded onto a 15% SDS-PAGE gel (PAGE Gel Rapid Preparation Kit, Shanghai Yase Biotechnology Co., Ltd, PG114) and electrophoresed at 150 V for 50 minutes. The separated proteins were then transferred to a PVDF membrane (22 860, Thermo Scientific, Rockford, USA) using a mini *trans*-blot cell (022 711, Bio-Rad, MA, USA) at 300 mA for 2 hours at 4 °C in transfer buffer (25 mM Tris pH 8.3, 192 mM glycine, 20% methanol). The PVDF membrane was blocked by incubating in 1% BSA prepared in Tris-buffered saline with Tween 20 (TBST: 20 mM Tris–HCl pH 7.6, 137 mM NaCl, 0.1% Tween 20) for 30 minutes at room temperature. It was then incubated with the primary nanobody (diluted in 1% BSA with 0.1% TBST, as specified in Table S2) overnight at 4 °C on a rocker. Following primary incubation, the membrane was washed three times with approximately 50 mL of TBST for 20 minutes per wash. In this detection scheme, the VHH–SpyTag nanobody first binds to the antigen on the membrane. The SpyTag then mediates the attachment of a polymeric structure. This polymer contains SnoopCatcher, which binds covalently to SnoopTag–biotin, thereby labeling the complex with biotin. The biotinylated complex is subsequently detected using streptavidin-conjugated horseradish peroxidase (SA-HRP) and visualized with ECL reagents. The membrane was incubated with ECL reagents at room temperature and the signal was captured on X-ray film (ProSignal Blotting Film, Genesee Scientific). For total protein visualization, the SDS-PAGE gel was stained directly by soaking in Coomassie Brilliant Blue (CBB) solution and then imaged on a light plate.

2.3 Affinity assessment of nanobodies *via* surface plasmon resonance (SPR)

The binding affinity of the nanobodies was evaluated using surface plasmon resonance (SPR) on a Biacore 8K instrument (Cytiva, USA). The COVID-19 nucleocapsid protein was immobilized on a sensor chip *via* amine coupling with EDC/NHS (1-ethyl-3-(3-dimethylaminopropyl) carbodiimide hydrochloride/*N*-hydroxysuccinimide). Binding kinetics for each nanobody were assessed at 25 °C by injecting six serial dilutions (ranging

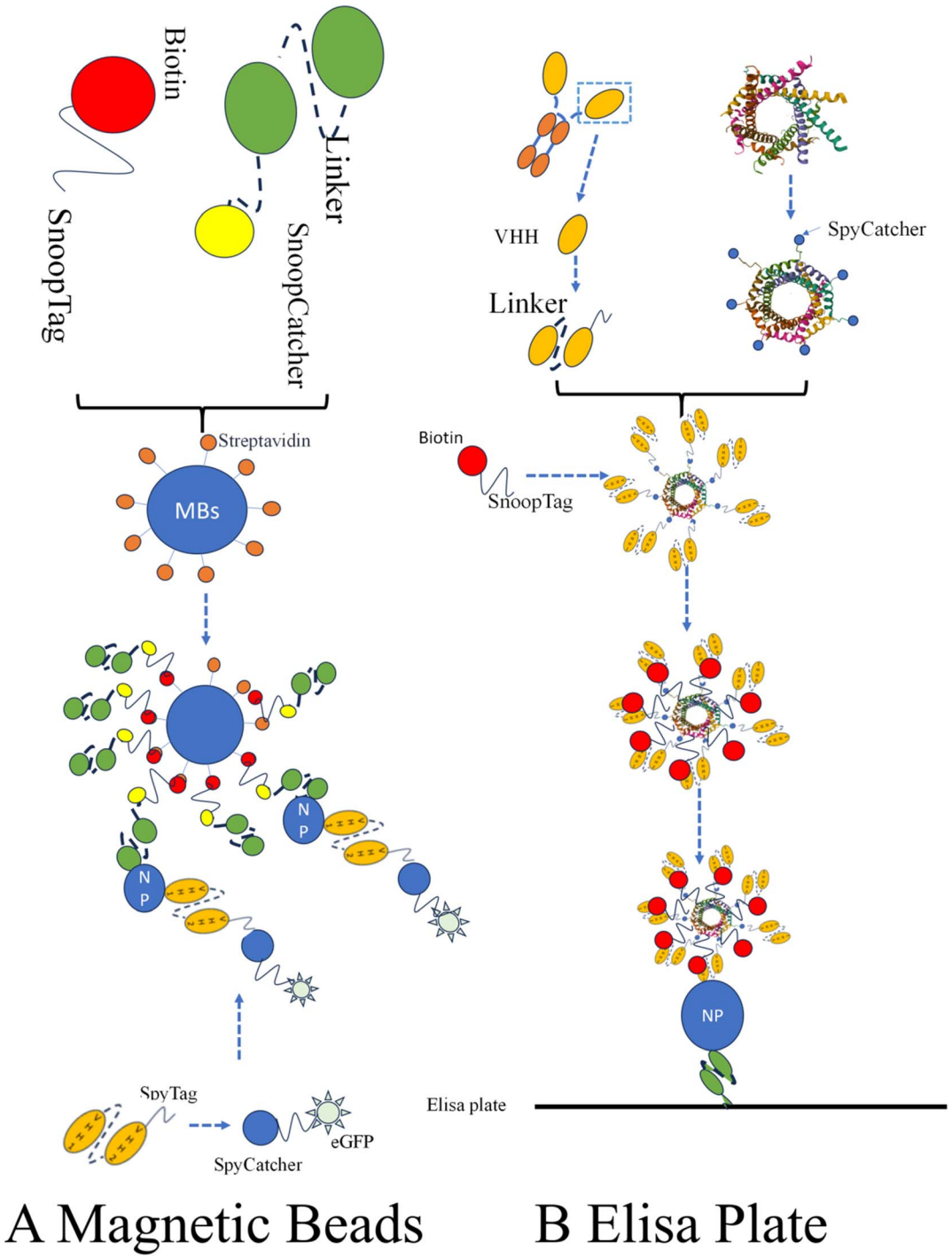

Fig. 1 Schematics of nanobody-based sandwich immunoassays for magnetic bead detection (A) and enzyme-linked immunosorbent assay (B). (A) Dimerized nanobodies were used to detect antigens in solution using magnetic beads, with eGFP-SpyCatcher serving as the fluorescent label. (B) Nanobodies were immobilized at the bottom of an ELISA plate to capture antigen proteins in solution. The recruitment of more biotin molecules through multimers, followed by amplification with streptavidin-HRP (SA-HRP), enabled the detection of lower antigen concentrations. We also attempted to use multimers in magnetic bead detection, but the specific affinity tags on the polymers that were recruited to different magnetic beads led to bead adhesion.

from 300 nM to 0 nM) over the antigen-coated surface at a flow rate of 100 μL min^{-1}. The dissociation phase was monitored for 600 seconds following each injection.

2.4 Antigen analysis with nanobody-conjugated magnetic beads

The Magnetic Bead (MB) sandwich immunoassay employs a biotinylated capture nanobody immobilized on MB and a paired, fluorescently labeled detection nanobody. To generate the

biotinylated capture nanobody, a tenfold molar excess of SnoopTag–biotin was incubated with the VHH–SnoopCatcher construct for 30 minutes to allow complete conjugation. Unreacted SnoopTag–biotin was removed using an ultrafiltration tube. For each assay, 300 ng of the resulting VHH–SnoopCatcher–SnoopTag–biotin conjugate was immobilized onto 100 μg of 2.8 μm streptavidin-MB (SA-MB, 10 mg mL; Biomagnetic Technology Co., Ltd, Wuxi, China). The MBs were then blocked by incubation with 1 mL of 1% BSA at 37 °C for 30 minutes. Following blocking, 400 ng of antigen was added to MBs according to the experimental groupings outlined in Fig. S1. A separate nanobody, serving as the detector, was fluorescently labeled as a VHH–SpyTag– > SpyCatcher–GFP construct. After each incubation step, which was performed for 30 minutes at room temperature, the MBs were separated from the solution using a magnetic rack (12321D, DynaMag, Thermo Fisher Scientific, USA) and washed three times with 1 mL of PBS. Binding events were confirmed by fluorescence microscopy at 400× total magnification, and images were acquired using a Nikon Ni_2 confocal microscope. The final immune-sandwich complex was structured as follows: MB–SA– > biotin–SnoopTag–SnoopCatcher–VHH– > NP– > VHH–SpyTag–SpyCatcher–GFP.

2.5 Antigen analysis with enzyme-linked immunosorbent assay (ELISA)

A sandwich Enzyme-Linked Immunosorbent Assay (ELISA) was subsequently employed to analyze the COVID-19 nucleocapsid

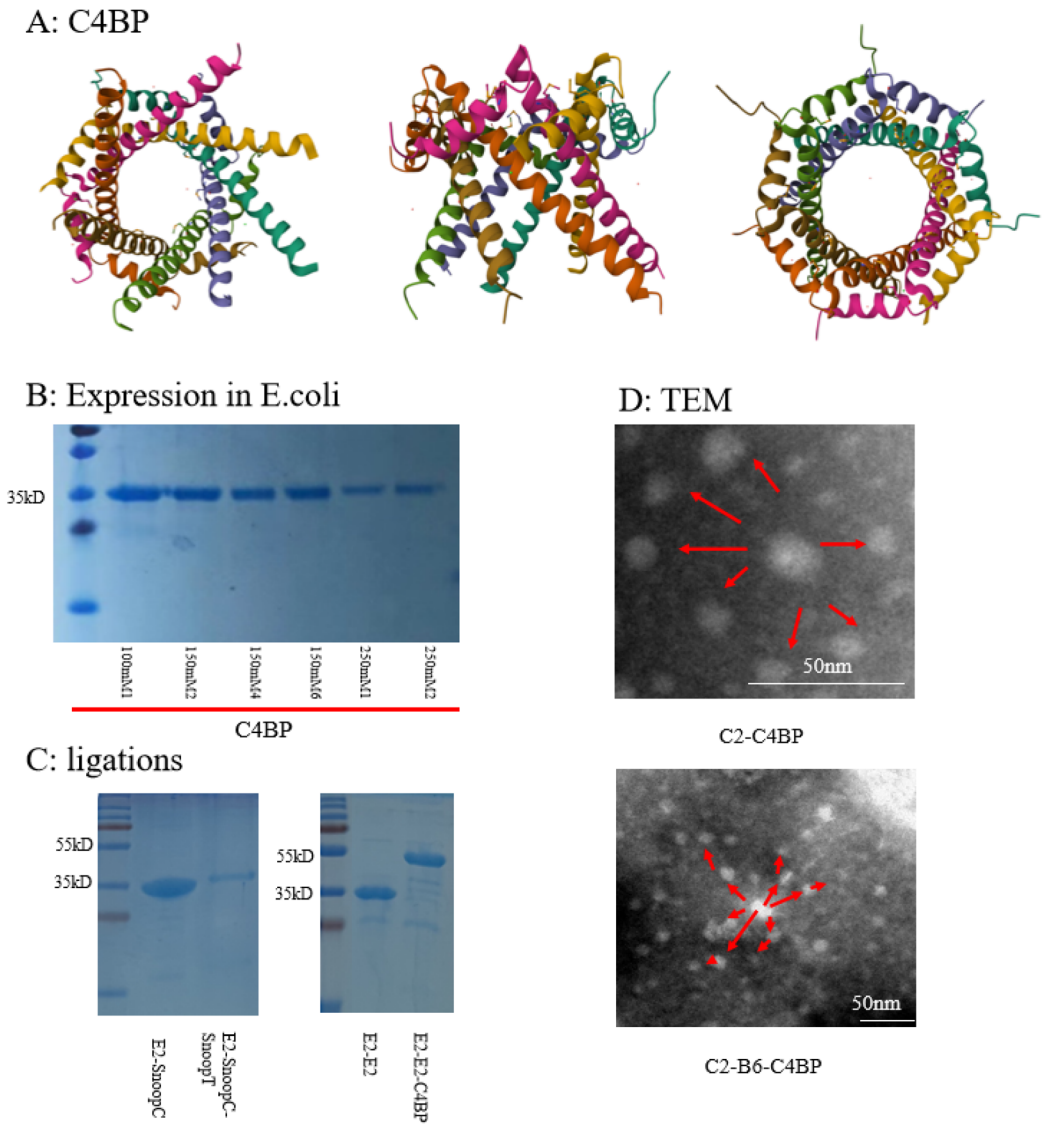

Fig. 2 Construction of the heptameric scaffold protein. (A) Schematic representation of the molecular structure of the C4BP heptamer (IMX313; PDB: 4B0F). Views from the bottom, side, and top are shown. The N-terminus is located at the top of the octopus-like structure. (B) Coomassie Blue-stained SDS-PAGE gel of purified heptameric C4BP samples. The scaffold protein SpyCatcher-C4BP-SnoopCatcher has a total molecular mass of 37 kD. (C) Analysis of nanobody biotinylation and polymerization. (Left) Biotinylation of E2-SnoopCatcher *via* conjugation to SnoopTag-Biotin, resulting in an approximate 2 kD shift and the formation of biotinylated E2-SnoopCatcher-SnoopTag-Biotin. (Right) Heptamerization of the dimeric nanobody E2-E2 by linkage to the C4BP scaffold. (D) Transmission electron microscopy (TEM) images of the C4BP scaffold bound to monomeric (C2) and dimeric (C2-B6) nanobodies.

protein. Unlabeled dimeric capture nanobodies (300 ng each of C2–B6 and E2–E2) were immobilized separately on polystyrene microplates (FST015, Beyotime Biotechnology, Shanghai, China). The coated plates were then blocked with 2% gelatin to prevent nonspecific binding. After blocking, the plates were washed three times with 250 μL of PBST for 5 minutes per wash. A gradient concentration series of COVID-19 nucleocapsid protein (0 to 10 μg mL^{-1}) was then gently added to the wells and incubated at room temperature for 1 hour. Following another PBST wash cycle, the plates were incubated with 100 μL of a prepared 200 μg per mL VHH–C4BP–biotin solution for 30 minutes. After a further wash step, 100 μL of a 1 : 2000 dilution of streptavidin-HRP (SA-HRP) conjugate was added to each well and incubated at room temperature for 30 minutes with gentle agitation. Finally, an ECL substrate was added to the wells for detection. The resulting signal was quantified using an ELISA microplate reader.

2.6 Statistical analysis

Data were analyzed by linear regression using GraphPad Prism 7. The limit of detection was defined as the mean absorbance of the blank control plus three standard deviations.

3 Result

3.1 Successful expression of nanobodies and polymeric scaffold protein

The molecular structure of the recombinant heptameric C4BP (IMX313: PDB, 4B0F) is shown in Fig. 2A. The purity of the polymer and its molecular weight of approximately 37 kD were confirmed by 15% SDS-PAGE (Fig. 2B). C4BP protein with high concentration and purity was collected and concentrated to 1 mg mL^{-1}. Nanobodies were pre-equipped with a SpyTag for subsequent linkage to the polymeric C4BP scaffold (Fig. 2C). For the immune-sandwich MBs and ELISA assays, capture nanobodies were biotinylated by conjugating VHH–SnoopCatcher to SnoopTag–biotin. The binding of the 12-amino-acid SnoopTag peptide results in an approximate 2 kD increase in the molecular weight of the biotinylated VHH (Fig. 2C). We further characterized the mono-heptamer (E2–C4BP) and dimer-heptamer (E2–E2–C4BP) constructs using transmission electron microscopy (TEM). The TEM images confirmed that the nanobody units extend radially from the central C4BP scaffold (Fig. 2D). To assess the solution-state properties of these megamolecules, we employed NanoTemper Panta plus (NanoTemper Technologies GmbH, Munich, Germany) to measure MicroScale Thermophoresis/Temperature-Related Intensity Change (MST/TRIC). This analysis verified the differentiation in the hydration sizes and diameters of the nanobodies and their polymers. Consistent with the TEM observations, we found that the hydrodynamic diameter increased with the molecular weight of the multipolymer complex (Fig. S3).

The antigen capture efficacy of the nanobodies was first validated by western blot (Fig. 3). The COVID-19 nucleocapsid protein was evenly loaded across six sample lanes. Three monomeric nanobodies (E2, C2, and B6) and two dimeric nanobodies (C2–B6 and E2–E2) all successfully bound the target antigen. This result confirmed that the macromolecular assembly, comprising immune recognition and biotin tagging *via* the VHH–SnoopCatcher–SnoopTag–Biotin system, proceeded successfully on the membrane. Interestingly, the staining intensity was stronger for monomeric nanobodies than for conventional antibodies. We hypothesize that under the conditions of antigen excess on the PVDF membrane, each antigen monomer binds one antibody molecule and carries one biotin label. In contrast, a dimeric nanobody, while capable of binding more antigen, would still be labeled with only one biotin molecule, resulting in a lower signal per antigen unit under these saturating conditions.

3.2 Polymerization-enhanced affinity of nanobodies

The affinity and kinetics of the recombinant nanobodies were evaluated by SPR (Fig. 4). Sensorgrams demonstrate that both dimeric and dimer-polymeric nanobodies interact robustly with the immobilized COVID-19 nucleocapsid protein (Fig. 4A). The

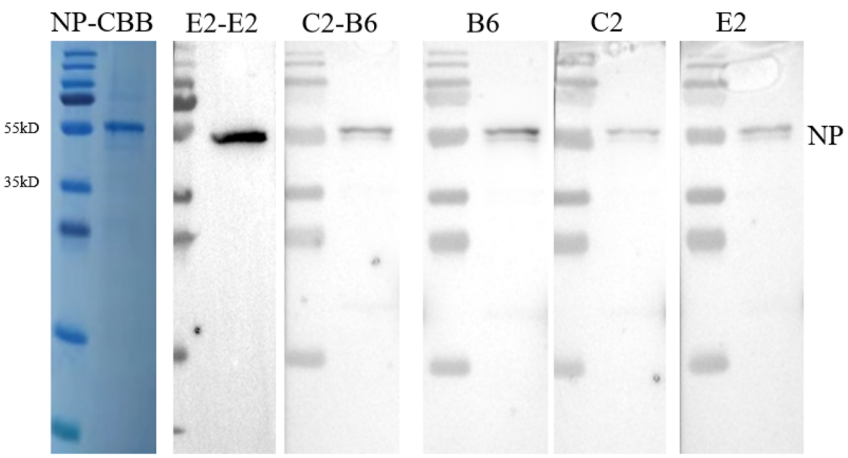

Fig. 3 Analysis of nanobody immunobinding and biotinylation using the heptameric scaffold protein. (Left) Coomassie Blue staining of the 55 kD SARS-CoV-2 nucleocapsid protein. (Right) The SARS-CoV-2 nucleocapsid protein was transferred to a PVDF membrane. Immunobinding activity was detected using the nanobody-C4BP-biotin complex *via* immunoblotting.

binding affinity of the dimeric and polymeric forms was substantially greater than that of the monomeric nanobodies (Fig. 4B). Furthermore, polymerization generally conferred a higher affinity than dimerization alone (Fig. 4C). When comparing the difference in binding affinity between dimers and heptamers, calculated as $[(-\log K_D, nM_1) - (-\log K_D, nM_2)]$, the heptamers consistently showed an increase of no less than 0.5 (~5 folds). This corresponds to an improvement of 0.5 to 1 order of magnitude for the E2 and C2 epitopes in their dimeric, heptameric, and 14-mer assemblies. Analysis of the kinetic parameters revealed distinct behaviors. For the C2–B6 construct, the association rate constants (k_a) of the dimer and polymer were not significantly different (4.95×10^4 *vs.* 7.54×10^4 1/Ms). However, the dissociation rate constant (k_d) of the polymer was markedly slower than that of the dimer (5.44×10^{-5} *vs.* 2.29×10^{-3} 1/s), indicating greatly improved complex stability. In contrast, for E2–E2, both the association (1.66×10^5 *vs.* 6.46×10^3 1/Ms) and dissociation (3.72×10^{-4} *vs.* 5.05×10^{-5} 1/s) parameters differed significantly between the dimer and polymer. We speculate that these differences arise from the distinct structural properties of their respective binding domains. The affinity of the polymeric nanobodies reached a level comparable to that of most murine-derived antibodies. Finally, we performed a cross-competition SPR assay. When a complementary dimeric nanobody was injected over an SPR sensorgram already saturated with the initial nanobody (either C2–B6 or E2–E2), a further increase in the binding response was observed (Fig. 4D). This indicates that C2–B6 and E2–E2 bind to

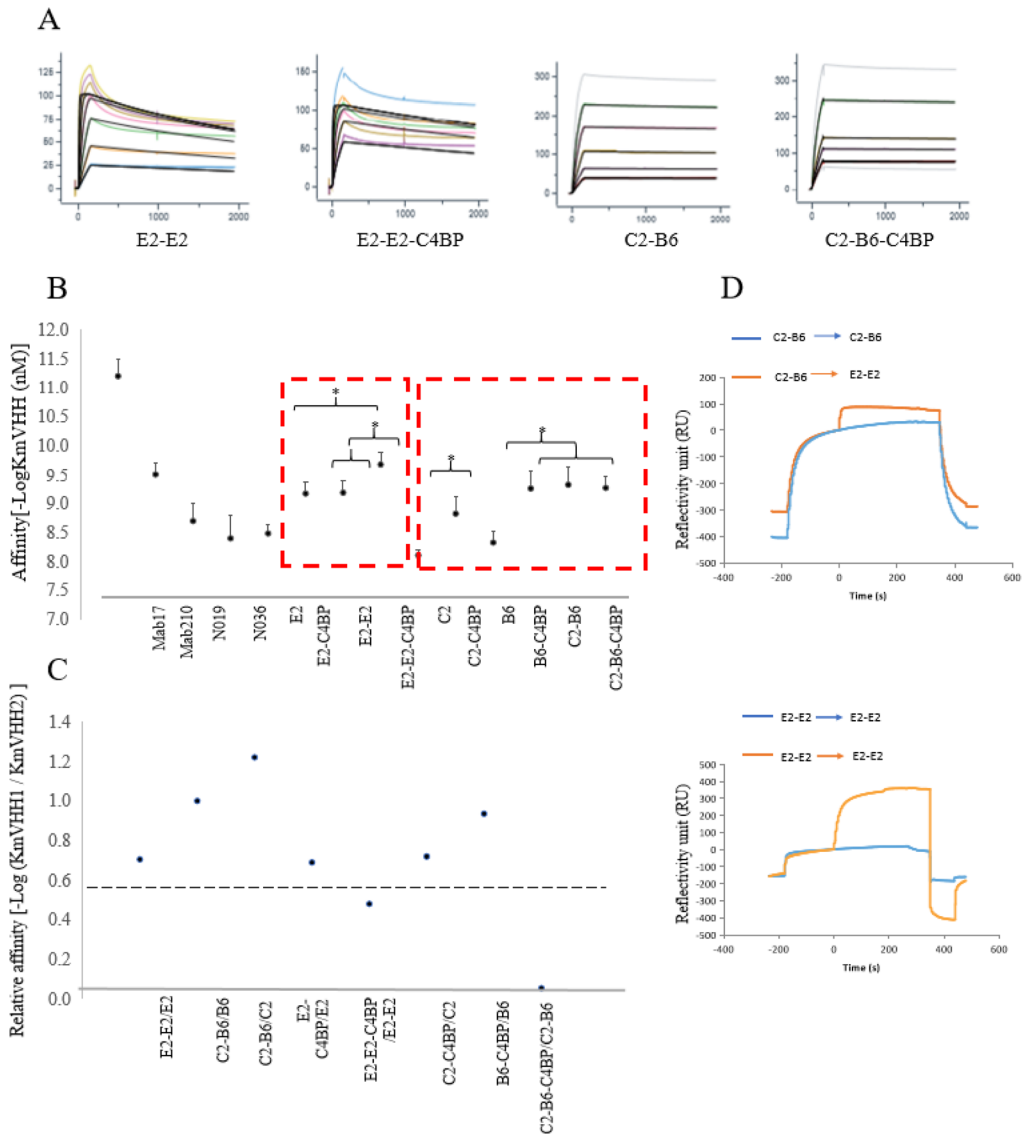

Fig. 4 Affinity analysis of recombinant polymers by surface plasmon resonance (SPR). (A) SPR sensorgrams with fitting curves for dimeric and polymeric nanobodies. (B) Affinity of monomers, dimers, and polymers, expressed as $-\log(K_D$, VHH [*nM*]). (C) Relative affinity comparison $[-\log(K_D$, VHH1/K_D, VHH2)] between dimers and heptamers. The dotted line indicates a 5-fold increase in KD. Dimerization and heptamerization significantly enhance nanobody affinity. (D) Epitope competition SPR analysis of the two dimeric nanobodies. E2–E2 and C2–B6 bind to non-overlapping antigen-binding sites. The blue dotted line marks the injection time of the second nanobody.

non-overlapping epitopes on the NP protein and can form a ternary complex simultaneously.

3.3 Nanobody immunological activity for immuno-sandwich analysis

To further validate the efficacy of nanobodies in identifying and capturing the COVID-19 nucleocapsid protein in solution, we performed a series of sandwich immunoassays (magnetic bead-based assay in Fig. 5 and ELISA in Fig. 6). In this design, the VHH–SnoopCatcher–SnoopTag–biotin pair served as the capture nanobody, immobilized on magnetic beads *via* streptavidin–biotin affinity, while fluorescently labeled nanobodies functioned as detection antibodies (forming the complex: MBs–SA– > biotin–VHH1– > NP– > VHH2–GFP). Initial experiments included blank and negative controls. The blank control consisted of untreated beads (Fig. 5A), while the negative control used beads with both E2 as the capture antibody and E2 as the detection antibody (Fig. 5B). In this negative control, the epitope for the detection antibody was blocked by the identical capture antibody, resulting in no detectable background signal from autofluorescence or nonspecific binding. Fig. 5C–F demonstrate that antigen captured by one

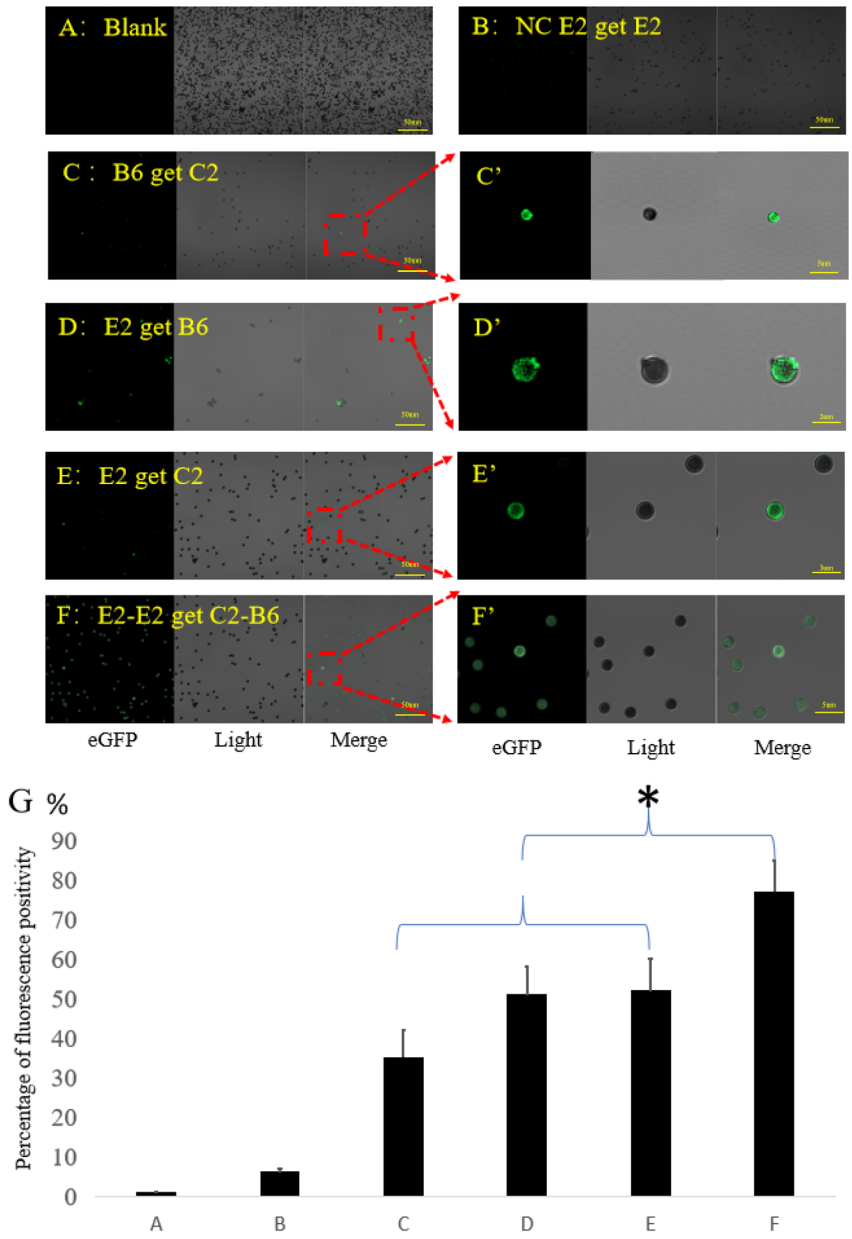

Fig. 5 Magnetic bead-based sandwich immunoassay. (A) Untreated magnetic beads (blank control). (B) Negative control using E2–biotin as the capture antibody and E2–GFP as the detection antibody. (C and C′) B6–biotin as the capture antibody and C2–GFP as the detection antibody. (D and D′) E2–biotin as the capture antibody and B6–GFP as the detection antibody. (E and E′) E2–biotin as the capture antibody and C2–GFP as the detection antibody. (F and F′) E2–E2-biotin as the capture antibody and C2–B6–GFP as the detection antibody. (G) Positive magnetic bead ratio intensity. *$P < 0.05$.

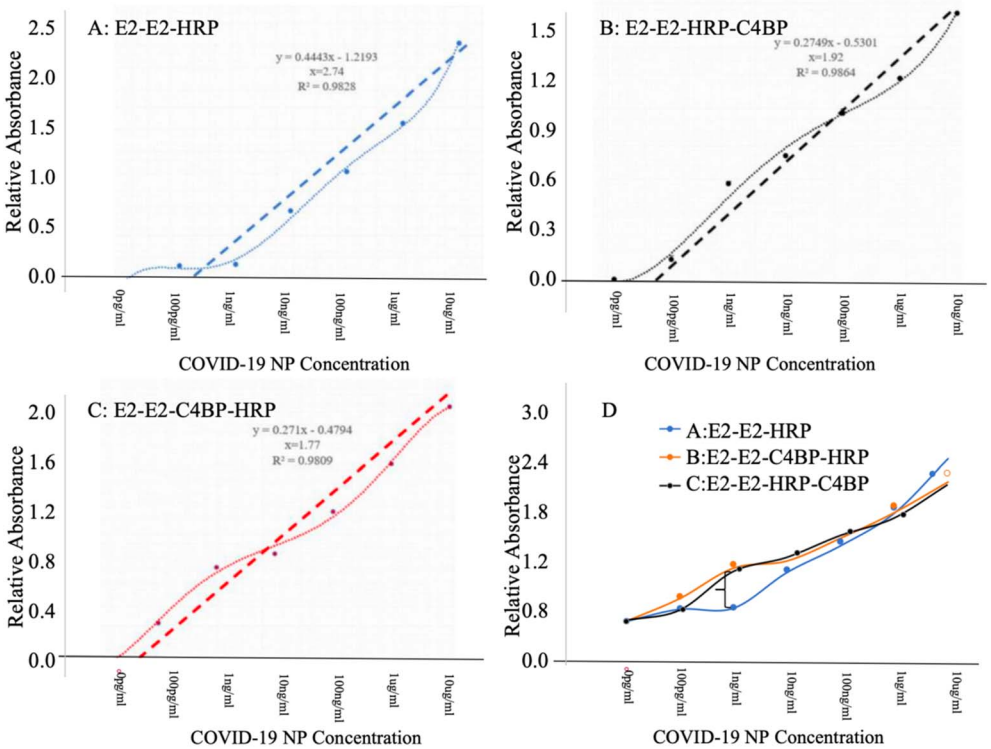

Fig. 6 Polymerized nanobody-based sandwich ELISA. (A–C) Schematics of the three different HRP conjugation methods. (A) HRP directly conjugated to the dimeric nanobody. (B) HRP first conjugated to C4BP, which is then linked to the SpyTag of the E2–E2 nanobody. (C) The nanobody is first combined with C4BP, and the complex is then labeled with HRP. (D) Comparison of the detection performance for the three labeling methods. The signal-to-noise ratio (log(S/N)) is shown on the *y*-axis.

monovalent nanobody does not occlude the epitopes recognized by other nanobodies, and each nanobody retains its ability to bind and generate a positive signal. Finally, we configured an immuno-sandwich assay using the dimer E2–E2 as the capture antibody and the dimer C2–B6 as the detection antibody for NP protein. This combination resulted in a stronger positive signal and a higher percentage of positive magnetic beads (Fig. 5G). Based on these results and our previous findings, we anticipate that employing dimeric and polymeric nanobodies in tandem will further enhance detection sensitivity.

The immuno-sandwich ELISA detection of soluble proteins is a prevalent method for diagnosing pathogenic infections. Theoretically, the C2–B6 dimer can bind a larger amount of antigen, whereas the E2–E2 dimer enables quicker and more stable biotin labeling of the antigen. Consequently, a heterologous system was developed, utilizing C2–B6 as the capture nanobody and E2–E2 as the detection nanobody. To enhance the affinity of this nanobody pair and amplify the biotin signal, C4BP was employed as a heptameric scaffold. Given that random conjugation of HRP to the polymers could alter nanobody function, two distinct polymer-labeling strategies were implemented. The first strategy involves assembling the nanobody and C4BP into a 14-mer complex, followed by the attachment of HRP to the polymeric nanobody (Fig. 6B). The alternative strategy first conjugates HRP to C4BP, which is subsequently linked to the nanobody, thereby avoiding potential occlusion of the nanobody's epitopes (Fig. 6C). The results from the three labeling groups were compared collectively (Fig. 6D). The vertical axis illustrates the signal-to-noise ratio (log(S/N)). We confirmed that both polymer-based approaches, whether the nanobody was conjugated before or after HRP labeling, significantly and indistinguishably enhanced the detection sensitivity of the nanobody. Ultimately, C4BP polymerization enhanced the limit of detection (LOD) for the COVID-19 nucleocapsid protein.

4 Discussion

Precise *in vitro* disease diagnosis is crucial for guiding clinical practice and fundamental research. Conventional Y-shaped antibodies have been extensively used in research, diagnostics, and therapeutics. However, their large size imposes limitations in certain applications, hindering delivery and access to internal antigenic epitopes.[32] The discovery of nanobodies has provided a dramatically smaller alternative. Nanobodies share significant sequence and structural similarity with the VH domain of human IgG3 apart from CH1. Their stability is partly determined by the CH2 domain, involving four key amino acids.[20] At approximately one-tenth the size of conventional antibodies, nanobodies represent the smallest known antigen-binding fragments and are commonly referred to as nanobodies. Nanobodies offer numerous advantages, including small size, high solubility, stability, strong specificity, ease of

genetic modification, straightforward expression and screening, and the capacity for further engineering. Their compact dimensions enable them to recognize concealed epitopes that are often inaccessible to traditional antibodies. These distinctive properties make nanobodies a prominent focus of scientific research.

In mammals, polymeric antibodies such as IgA and IgM temporarily enhance immune affinity during acute infections.[33] Protein engineering is a pivotal tool across industrial, therapeutic, and research applications[34]—enabling the development of antibody fusion proteins,[35] the design of biomaterials with tailored scaffold matrices and functional groups,[36] and the regulation of gene expression *via* DNA-binding repressors or activators.[37] Most fusion proteins are genetically encoded constructs connected by flexible, rigid, or cleavable linkers.[38] Beyond monovalent nanobodies, current research is exploring bivalent, bispecific, and other fusion protein formats to improve their target specificity and binding affinity, thereby enhancing their therapeutic potential.[39] Binding modules have been utilized to develop chimeric protein therapies based on antibodies.[40] For example, antibody-enzyme conjugates have been designed as site-selectively activated prodrugs, such as suicide domains for cancer therapy, where antibodies serve as targeting moieties.[40] A dual-labeled recombinant antibody targeting EGFR molecules has demonstrated superior tumor growth suppression compared to a bivalent monospecific antibody.[41] While covalent *in vitro* assembly can form permanent protein linkages, the inherent limitations of current ligation systems constrain the variety of molecular topologies that can be achieved. Sortase- and intein-mediated ligations are restricted to connections between the N- and C-termini of target proteins. The C4-binding protein (C4BP) features an octopus-like structure composed of seven α-chains,[29] with a C-terminal amphipathic helix and two cysteine residues that are well characterized for their role in polymerization.[27] Achieving complex molecular architectures requires modular assemblies incorporating multiple interacting domains. This goal can be partially realized using two orthogonal protein pairs, SpyTag/SpyCatcher and SnoopTag/SnoopCatcher, integrated into the C-terminal display platform of C4BP, thereby enabling extensive molecular assembly.[42] Our study presents a novel platform that combines an N-terminal dimeric nanobody on C4BP with a C-terminal biotin modification *via* an isopeptide bond, creating a bifunctional tool for both high-affinity nanobody tracing and sensitive signal detection. The scaffold protein SpyCatcher–C4BP–SnoopCatcher has a total molecular weight of 37 kD (Fig. S2). We used a pure, homogeneous protein sample at a high concentration (10 mg mL^{-1}) to facilitate sandwich immunoassays. The combination of C4BP and the E2–E2 dimer produces a distinct band at approximately 75 kD (Fig. 2C, right). Fig. 2D shows the heptamer (C2–C4BP), dimers, and dimer-heptamer complexes (C2–B6–C4BP) visualized by TEM. We also measured the hydration diameter of the proteins using NanoTemper. The hydrodynamic diameter of the macromolecules also increases with molecular stacking and higher molecular weight (Fig. S3).

We initially confirmed nanobody activity by western blot analysis (Fig. 3). The COVID-19 NP antigen was immobilized on a PVDF membrane and probed with VHH–SpyTag. SpyCatcher–C4BP–SnoopCatcher was then added, followed by SnoopTag–biotin to biotinylate the complex. Finally, streptavidin-HRP (SA-HRP) was applied to detect specific binding. Our nanobodies successfully bound to the membrane-immobilized antigen and produced a positive HRP signal. These results preliminarily verify that the nanobody retains its immunoreactivity on PVDF membranes and can function effectively as a antigen detection in western blot assays.

Affinity is a critical parameter for evaluating antibody performance. We assessed the antigen-binding capability of the recombinant polymers using SPR on a Biacore 8K instrument,[43] which represents the most direct method for determining protein affinity characteristics (Fig. 4). The COVID-19 nucleocapsid protein was covalently immobilized on the sensor chip channels. The recombinant dimers and polymers demonstrated substantially higher affinity than their monomeric counterparts (Fig. 4B and C). Monomeric nanobodies (E2, C2, B6) exhibited affinities ranging from 10^{-7} to 10^{-8} M, which improved by 1–2 orders of magnitude (10–100 fold) through dimerization and polymerization strategies (Fig. 4B). The C2–B6 dimer showed particularly significant enhancement, exceeding one order of magnitude improvement over the C2 and B6 monomers (Fig. 4C). Overall, all dimeric constructs demonstrated 0.5 to 1.5 orders of magnitude (5–50 fold) higher affinity than their monomeric forms. Consistent with previous research, both heptameric structures and heptamerized dimeric structures showed significantly enhanced affinity. This enhancement likely results from the polymeric architecture, which clusters multiple nanobodies to simultaneously engage antigens and anchor more signaling molecules, thereby amplifying the overall binding strength. In SPR-based epitope competition experiments where dimers C2–B6 and E2–E2 served as capture nanobodies, both effectively bound to the positive control (Fig. 4D). We observed that E2–E2 exhibited faster binding kinetics regardless of injection order, while C2–B6 demonstrated higher antigen-carrying capacity. Based on these epitope competition results, we infer that employing C2–B6 as a capture nanobody increases signal density, while using E2–E2 as the detection antibody provides rapid and stable antigen binding, together enhancing overall detection sensitivity.

To detection the concentration of antigen in solution, we conducted immune-sandwich assay with MBs and Elisa. To prevent nonspecific aggregation of magnetic beads in the absence of antigen, we implemented the VHH–SnoopCatcher and SnoopTag–biotin system for site-specific biotinylation of dimeric nanobodies in the sandwich immunoassay (Fig. 5). Conjugation *via* the SnoopCatcher/SnoopTag system resulted in an approximate 2 increase in molecular weight (Fig. 2C). The absence of additional bands confirmed complete reaction between SnoopCatcher and SnoopTag–biotin. The use of excess SnoopTag ensured efficient biotinylation of all SnoopCatcher fusion proteins. Our results demonstrate effective nanobody function in solution-phase magnetic bead assays. As anticipated, no fluorescence signal was observed in either the blank

control (untreated magnetic beads, Fig. 5A) or the negative control. In the negative control, when all antigen binding sites were occupied by the capture antibody, the fluorescently labeled detection antibody of the same specificity could not form additional immune complexes (E2-coated beads with E2 detection antibody, Fig. 5B). All other test groups showed the expected positive fluorescence signals (Fig. 5C–F), with the two paired dimeric nanobodies exhibiting stronger affinity than other combinations. We subsequently applied the polymeric nanobody-based sandwich ELISA for detecting antigen in solution. Two unlabeled dimeric nanobodies, C2–B6 and E2–E2 (Fig. S2), were separately immobilized on microplates as capture antibodies (VHH1). The plates were then incubated with COVID-19 nucleocapsid protein followed by detection nanobodies (VHH2), each for 30 minutes. To improve the detection limit for NP, we employed C4BP as a heptameric scaffold to recruit multiple detection antibodies and amplify the fluorescence signal, thereby enhancing ELISA sensitivity. The limit of detection was determined by calculating the signal-to-noise ratio (Fig. 6). In this configuration, C2–B6 served as the capture nanobody while the E2–E2–C4BP dimer-heptamer (14-mer) acted as the biotinylated detection reagent. Both the C2–B6–C4BP and E2–E2–C4BP dimer-heptamers enhanced the detection limit by more than tenfold (Fig. 6). We propose that this enhanced sensitivity results not only from improved binding affinity but also from the heptamer's capacity to concentrate multiple biotin tags, thereby amplifying the detection signal. This signal amplification effectively lowers the detection limit, enabling earlier identification of infected individuals and facilitating timely therapeutic intervention.

Although nanobody applications are becoming increasingly widespread,[12] their affinity often remains inferior to that of conventional antibodies. Optimizing nanobodies typically requires combined approaches of sequence engineering and structural modification to validate improvement strategies. Key research directions include elucidating antigen–antibody binding interfaces and conjugation strategies, developing artificial directed evolution platforms for nanobody sequences, and establishing more accessible naive affinity libraries. These efforts aim to enhance antibody affinity, improve antigen detection sensitivity, and achieve more efficient antigen capture.

In this study, we developed a smart modular system using the C4BP heptameric scaffold that simultaneously displays seven N-terminal VHH domains and seven C-terminal biotin tracers. This dimer-heptamer configuration creates a 14-valent display platform designed to enhance nanobody avidity and amplify signals in sandwich immunoassays. Our results demonstrate over tenfold improvement in detection sensitivity for COVID-19 nucleocapsid protein in both magnetic bead and ELISA systems. This modular covalent-noncovalent 14-mer system represents a promising toolkit for rapidly developing highly sensitive detection platforms for pathogen antigens during early infection stages.

Author contributions

F. Wang and L.-J. Huo conceived the study and participated in all experiments. F. Wang, J. Chen, and J.-H. Chen performed protein production and the magnetic bead immuno-sandwich assay. F. Wang constructed the plasmid. L.-Q. Hu provided automated instrumentation support for protein TEM and immunoassays.

Conflicts of interest

The authors declare that they have no conflicts of interest.

Data availability

The data that support the findings of this study are available from the corresponding author upon reasonable request.

Supplementary information (SI) is available. See DOI: https://doi.org/10.1039/d5ra03619d.

Acknowledgements

This work was supported by Faculty Development Grants from Hubei University of Medicine (2025QDJZR01).

References

1 R. Janssens, S. Dekker, R. W. Hendriks, G. Panayotou, A. V. Remoortere, J. K.-A. San, F. Grosveld and D. Drabek, *Proc. Natl. Acad. Sci. U. S. A.*, 2006, **103**, 15130–15135, DOI: 10.1073/pnas.0601108103.

2 C. Hamers-Casterman, T. Atarhouch, S. Muyldermans, G. Robinson, C. Hammers, E. B. Songa, N. Bendahman and R. Hammers, *Nature*, 1993, **363**, 446–448, DOI: 10.1038/363446a0.

3 A. de Marco, *Protein Expr. Purif.*, 2020, **172**, 105645, DOI: 10.1016/j.pep.2020.105645.

4 A. S. Greenberg, D. Avila, M. Hughes, A. Hughes, E. C. McKinney and M. F. Flajnik, *Nature*, 1995, **374**, 168–173, DOI: 10.1038/374168a0.

5 M. Arbabi-Ghahroudi, *Int. J. Mol. Sci.*, 2022, **23**, 5009, DOI: 10.3390/ijms23095009.

6 L. Zhang, Y. F. Lin, L. Hu, Y. N. Wang, C. H. Hu, X. Y. Shangguan, S. Z. Tang, J. C. Chen, P. Hu, Z. S. Chen, Z. F. Ke and Z. Chen, *Mol. Cancer*, 2025, **24**, 119, DOI: 10.1186/s12943-025-02253-6.

7 S. Yi, K. Noh, H. Kim, E. Jung, S. Kim, J. U. Lee, K. Guk, J. Choi, E. K. Lim, S. Kim, H. Park, J. H. Lim, C. R. Jung, T. Kang and J. Jung, *Mol. Cancer*, 2025, **24**, 124, DOI: 10.1186/s12943-025-02325-7.

8 M. Maltseva, M. A. Rossotti, J. Tanha and M. A. Langlois, *Viruses*, 2025, **17**, 571, DOI: 10.3390/v17040571.

9 R. Chakravarty, S. Goel and W. Cai, *Theranostics*, 2014, **4**, 386–398, DOI: 10.7150/thno.8006.

10 V. K. Nguyen, A. Desmyter and S. Muyldermans, *Adv. Immunol.*, 2001, **79**, 261–296, DOI: 10.1016/s0065-2776(01)79006-2.

11 S. McRae, in *Mechanisms of Vascular Disease: A Reference Book for Vascular Specialists*, ed. R. Fitridge and M. Thompson, Adelaide (AU), 2011, https://www.ncbi.nlm.nih.gov/pubmed/30485009.
12 G. Hassanzadeh-Ghassabeh, N. Devoogdt, P. De Pauw, C. Vincke and S. Muyldermans, *Nanomedicine*, 2013, **8**, 1013–1026, DOI: 10.2217/Nnm.13.86.
13 B. A. Keyt, R. Baliga, A. M. Sinclair, S. F. Carroll and M. S. Peterson, *Antibodies*, 2020, **9**, 53, DOI: 10.3390/antib9040053.
14 T. Uchanski, S. Masiulis, B. Fischer, V. Kalichuk, U. López-Sánchez, E. Zarkadas, M. Weckener, A. Sente, P. Ward, A. Wohlkönig, T. Zögg, H. Remaut, J. H. Naismith, H. Nury, W. Vranken, A. R. Aricescu, E. Pardon and J. Steyaert, *Nat. Methods*, 2021, **18**, 60, DOI: 10.1038/s41592-020-01001-6.
15 N. Nuñez-Prado, M. Compte, S. Harwood, A. Alvarez-Méndez, S. Lykkemark, L. Sanz and L. Alvarez-Vallina, *Drug Discovery Today*, 2015, **20**, 588–594, DOI: 10.1016/j.drudis.2015.02.013.
16 L. Santambrogio and H. G. Rammensee, *Immunogenetics*, 2019, **71**, 203–216, DOI: 10.1007/s00251-018-1093-z.
17 R. Y. P. Lue, G. Y. J. Chen, Y. Hu, Q. Zhu and S. Q. Yao, *J. Am. Chem. Soc.*, 2004, **126**, 1055–1062, DOI: 10.1021/ja037914g.
18 D. A. Levary, R. Parthasarathy, E. T. Boder and M. E. Ackerman, *PLoS One*, 2011, **6**, e18342, DOI: 10.1371/journal.pone.0018342.
19 S. M. Deyev and E. N. Lebedenko, *Bioessays*, 2008, **30**, 904–918, DOI: 10.1002/bies.20805.
20 O. H. Laitinen, H. R. Nordlund, V. P. Hytönen and M. S. Kulomaa, *Trends Biotechnol.*, 2007, **25**, 269–277, DOI: 10.1016/j.tibtech.2007.04.001.
21 A. Ferreira, M. Takahashi and V. Nussenzweig, *J. Exp. Med.*, 1977, **146**, 1001–1018, DOI: 10.1084/jem.146.4.1001.
22 K. D. Brune, C. M. Buldun, Y. Y. Li, I. J. Taylor, F. Brod, S. Biswas and M. Howarth, *Bioconjugate Chem.*, 2017, **28**, 1544–1551, DOI: 10.1021/acs.bioconjchem.7b00174.
23 B. Zakeri, J. O. Fierer, E. Celik, E. C. Chittock, U. Schwarz-Linek, V. T. Moy and M. Howarth, *Proc. Natl. Acad. Sci. U. S. A.*, 2012, **109**, E690–E697, DOI: 10.1073/pnas.1115485109.
24 W. B. Zhang, F. Sun, D. A. Tirrell and F. H. Arnold, *J. Am. Chem. Soc.*, 2013, **135**, 13988–13997, DOI: 10.1021/ja4076452.
25 J. O. Fierer, G. Veggiani and M. Howarth, *Proc. Natl. Acad. Sci. U. S. A.*, 2014, **111**, E1176–E1181, DOI: 10.1073/pnas.1315776111.
26 G. Veggiani, T. Nakamura, M. D. Brenner, R. V. Gayet, J. Yan, C. V. Robinson and M. Howarth, *Proc. Natl. Acad. Sci. U. S. A.*, 2016, **113**, 1202–1207, DOI: 10.1073/pnas.1519214113.
27 T. Hofmeyer, S. Schmelz, M. T. Degiacomi, M. Dal Peraro, M. Daneschdar, A. Scrima, J. van den Heuvel, D. W. Heinz and H. Kolmar, *J. Mol. Biol.*, 2013, **425**, 1302–1317, DOI: 10.1016/j.jmb.2012.12.017.
28 B. Valldorf, H. Fittler, L. Deweid, A. Ebenig, S. Dickgiesser, C. Sellmann, J. Becker, S. Zielonka, M. Empting, O. Avrutina and H. Kolmar, *Angew. Chem., Int. Ed.*, 2016, **55**, 5085–5089, DOI: 10.1002/anie.201511894.
29 Z. F. Li, Y. Wang, N. Vasylieva, D. B. Wan, Z. H. Yin, J. X. Dong and B. D. Hammock, *Anal. Chem.*, 2020, **92**, 10083–10090, DOI: 10.1021/acs.analchem.0c01908.
30 S. A. Ogun, L. Dumon -Seignovert, J. B. Marchand, A. A. Holder and F. Hill, *Infect. Immun.*, 2008, **76**, 3817–3823, DOI: 10.1128/Iai.01369-07.
31 G. P. Anderson, J. L. Liu, T. J. Esparza, B. T. Voelker, E. R. Hofmann and E. R. Goldman, *Anal. Chem.*, 2021, **93**, 7283–7291, DOI: 10.1021/acs.analchem.1c00677.
32 L. F. Wang, X. L. Liu, X. K. Zhu, L. Wang, W. Wang, C. Z. Liu, H. L. Cui, M. Y. Sun and B. Gao, *Protein Eng. Des. Sel.*, 2013, **26**, 417–423, DOI: 10.1093/protein/gzt011.
33 A. Mullard, *Nat. Rev. Drug Discovery*, 2017, **16**, 810, DOI: 10.1038/nrd.2017.211.
34 J. L. Foo, C. B. Ching, M. W. Chang and S. S. J. Leong, *Biotechnol. Adv.*, 2012, **30**, 541–549, DOI: 10.1016/j.biotechadv.2011.09.008.
35 P. J. Carter, *Exp. Cell Res.*, 2011, **317**, 1261–1269, DOI: 10.1016/j.yexcr.2011.02.013.
36 R. L. DiMarco and S. C. Heilshorn, *Adv. Mater.*, 2012, **24**, 3923–3940, DOI: 10.1002/adma.201200051.
37 A. J. Bogdanove and D. F. Voytas, *Science*, 2011, **333**, 1843–1846, DOI: 10.1126/science.1204094.
38 X. Y. Chen, J. L. Zaro and W. C. Shen, *Adv. Drug Delivery Rev.*, 2013, **65**, 1357–1369, DOI: 10.1016/j.addr.2012.09.039.
39 Q. Kong, Y. Yao, R. Chen and S. Lu, *Sheng Wu Gong Cheng Xue Bao*, 2014, **30**, 1351–1361, https://www.ncbi.nlm.nih.gov/pubmed/25720150.
40 M. M. Harmsen and H. J. De Haard, *Appl. Microbiol. Biotechnol.*, 2007, **77**, 13–22, DOI: 10.1007/s00253-007-1142-2.
41 R. C. Roovers, M. J. W. D. Vosjan, T. Laeremans, R. el Khoulati, R. C. G. de Bruin, K. M. Ferguson, A. J. Verkleij, G. A. M. S. van Dongen and P. M. van Bergen en Henegouwen, *Int. J. Cancer*, 2011, **129**, 2013–2024, DOI: 10.1002/ijc.26145.
42 L. L. Tan, S. S. Hoon and F. T. Wong, *PLoS One*, 2016, **11**, e0165074, DOI: 10.1371/journal.pone.0165074.
43 E. Britti, F. Delaspre, J. Tamarit and J. Ros, *Neuronal Signaling*, 2018, **2**, NS20180061.